Journal of Hazardous Materials 457 (2023) 131692

Contents lists available at ScienceDirect

Journal of Hazardous Materials

journal homepage: www.elsevier.com/locate/jhazmat

Research Paper

Remobilization characteristics and diffusion kinetic processes of sediment zinc (Zn) in a tidal reach of the Pearl River Estuary, South China

Lei Gao [a,*], Rui Li [b], Zuobing Liang [b], Chenchen Yang [b], Zaizhi Yang [b], Lei Hou [c], Lei Ouyang [a], Xiuhua Zhao [a], Jianyao Chen [b], Ping Zhao [a]

[a] Key Laboratory of Vegetation Restoration and Management of Degraded Ecosystems, South China Botanical Garden, Chinese Academy of Sciences, Guangzhou 510650, China
[b] School of Geography and Planning, Sun Yat-Sen University, Guangzhou 510275, China
[c] College of Ecology and Environment, Southwest Forestry University, Kunming 650224, China

HIGHLIGHTS

- Diagenesis decoupled Zn release and reductive dissolution of Fe/Mn oxides in sediment.
- Organically complexed Zn was turned into ion and inorganic complexes with raising TDS.
- DIFS model revealed high resupply rate of Zn from sediment solid phase to porewater.
- Sediment acted as a source of Zn to freshwater and as a sink in brackish water zone.

GRAPHICAL ABSTRACT

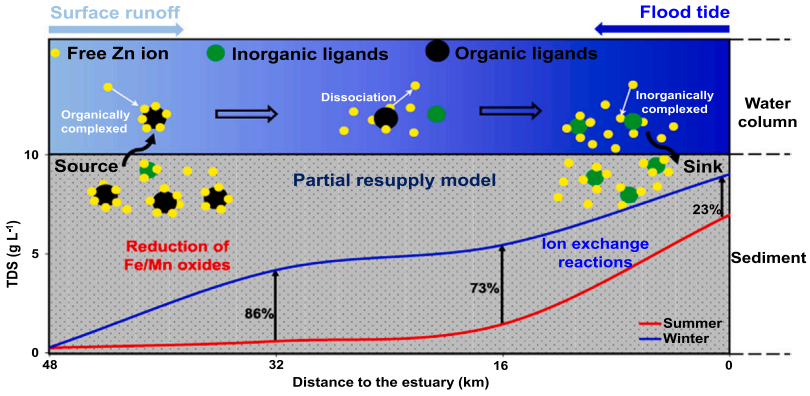

ARTICLE INFO

Editor: Dr. Y Deng

Keywords:
Saltwater-freshwater interzone
Zn speciation
Resupply capacity
Diffusive flux
Source/sink phases

ABSTRACT

Exploration of the remobilization mechanism of trace metals in estuarine sediments remain challenging because of dynamic hydrochemical conditions. This study integrated a chemical sequential extraction procedure (BCR), the diffusive gradient in thin films (DGT) and high-resolution dialysis techniques, and Visual MINTEQ ver.3.1 to identify the seasonal mobilization characteristics of sediment Zn within a tidal reach, South China. The mobility of sediment Zn based on the BCR procedure contradicted the results of DGT analysis. In summer, reductive dissolution of Fe/Mn oxides was the key driver of sediment Zn remobilization; during winter, cation exchange reactions facilitated the mobilization of Zn in the brackish water zone. The time-dependence ratios of DGT-labile Zn and dissolved Zn concentrations (mean: 0.34–0.81) indicated the sediment solid phase had partially sustained capacity to resupply Zn to the porewater in both seasons. Sediments generally functioned as a source of Zn in the freshwater zone with organically complexed Zn being diffusively released into the water column at rates of 0.3–15.5 $\mu g \cdot m^{-2} \cdot d^{-1}$. In the brackish water zone, the dominant Zn species were transformed into free Zn ions and

* Corresponding author.
E-mail address: nvtoo@sina.com (L. Gao).

https://doi.org/10.1016/j.jhazmat.2023.131692
Received 13 March 2023; Received in revised form 24 April 2023; Accepted 22 May 2023
Available online 24 May 2023

Zn–inorganic complexes and migrated into sediment, with respective influxes of 18.9–70.7 $\mu g \cdot m^{-2} \cdot d^{-1}$ and 18.9–68.3 $\mu g \cdot m^{-2} \cdot d^{-1}$, which shifted to a sink of Zn.

1. Introduction

Zinc (Zn) is one of the most abundant metal elements in the Earth's crust and is ubiquitous in environmental media (i.e., water, soil, and atmosphere) [36]. Trace Zn is essential to the growth and development of all organisms [7]. When the Zn concentration exceeds a certain limit, water becomes metallic in taste and aquatic organisms experience various acute or chronic toxic effects [33]. Due to its distinctive physicochemical properties including stability, non-degradability, and persistence in environmental media, Zn readily undergoes bioaccumulation and biomagnification in the food chain, thereby threatening human health [13,50].

In aquatic environments, Zn primarily originates from the weathering of parent rocks and discharge from anthropogenic activities; it tends to be adsorbed on suspended particulate matter and then deposited in sediment, which generally acts a major sink for trace metals in river basins [15,27]. However, rather than serving as the ultimate destination of buried metals, sediment is an important site for the initiation of physical and biogeochemical cycles. Driven by hydraulic disturbances, sediment solid-bound metal can be resuspended into the water column; furthermore, because of changes in physicochemical properties of the water column and sediment followed by redistribution of sediment metals between the solid and liquid phases, the formation of a concentration gradient at the sediment–water interface (SWI) is regarded as a key factor that drives the diffusive release of sediment metals into the overlying water [5,12]. Under such conditions, the sediment serves as a major source of metals, probably leading to secondary contamination of the water column and risking to aquatic ecosystems.

The mobility of Zn is largely dependent on its remobilization/immobilization mechanisms and its chemical speciation in sediment, both of which are closely associated with diverse factors during geochemical cycling processes. Alkaline conditions enable the accumulation and immobilization of metals in sediments, whereas acidification and increases in ionic strength apparently enhance the mobility of metals [11]. Additionally, a reducing environment is usually formed because of dissolved oxygen depletion, which is induced by the mineralization of organic matter (OM) in sediment [47]. Then, successive reduction of Fe/Mn oxides and sulfates occurs in the ideal order of reduction reactions in anaerobic sediments [11,12]. Importantly, the decomposition of OM and reductive dissolution of Fe/Mn oxides have been identified as the main contributors to Zn release from sediment solids into the porewater [15]. However, sustained development of reducing conditions can cause sulfides that originate from the reduction of sulfates to bind remobilized Zn, thereby forming insoluble zinc sulfide minerals (ZnS) and substantially decreasing Zn mobility [6,32]. In contrast, sulfide oxidation may occur because of anaerobic sediment resuspension, leading to Zn remobilization. Nevertheless, Fe oxides formed during the resuspension process act as efficient scavengers, largely sequestering the remobilized Zn [11,16]. The migration and immobilization behaviors of Zn are extremely sensitive to dynamic oxidation–reduction cycles in sediment.

Conventional research methods generally produce analytical errors because of changes in the chemical properties of sediment samples during transportation, storage, and pretreatment. Novel in situ passive sampling techniques (e.g., diffusive gradients in thin film [DGT] and high-resolution dialysis [HR-Peeper]) can overcome these deficiencies and have been widely used to explore the remobilization mechanisms of Zn in riverine, lacustrine, and estuarine sediments [15,26,41,47]. Based on the passive sampling and subsequent comprehensive physico-chemical analysis of sediment porewater, a thermodynamic chemical equilibrium models (e.g., Visual MINTEQ and WHAM) can be applied to simulate the concentrations and relative proportions of various metal species, including free ions and both inorganically and organically complexed metals; they can also estimate the diagenesis extent of a specific metal mineral based on the saturation index in solution [22,38,6]. The integration of DGT measurements with modeled metal speciation can provide insights into the composition of labile metals and remobilization mechanisms of sediment metals [14]. As a dynamic sampling method, the DGT probe captures target metals from labile fractions in porewater and from the solid phase. Consequently, the DGT Induced Fluxes in Sediments and Soils (DIFS) model was developed to describe the resupply kinetics of a specific metal from the solid to dissolved phases and to quantitatively determine the remobilization potentials of sediment metals [23,44,47,8]. To ascertain the source/sink relationships of a specific chemical substance between sediment and the water column, the Fick's first law of diffusion is regarded as a powerful tool for identifying its migration direction and the estimation of diffusive fluxes across the SWI [4]. Moreover, several literatures reported that sediment generally acted as a source of metals in freshwater bodies during summer seasons because of stronger reductive dissolution of Fe/Mn oxides; which then shifted to a sink in winter [15,39–41,43]. However, due to the differences in the diffusion rates of free metals and their organic complexes in aqueous environments [48], diffusive flux estimation based on the total concentration of dissolved metals and the unified diffusion coefficients will be problematic, likely leading to substantial prediction errors. More importantly, knowledge gaps still exist for spatiotemporal variations in remobilization characteristics, speciation and source/sink phases of trace metals at the SWI in estuarine regions as a result of highly dynamic hydrochemical conditions.

The Pearl River (PR) delta is among the most developed areas in China after experiencing four decades of urbanization and industrialization since the reform and opening up in 1978. According to the sedimentary records in the PR estuary, increased contamination loads were found before 2000; and then Zn loads of surface runoff showed a gradually decreasing trend over the past 10 years [28,45]. Previous reports have indicated that Zn accumulation occurred in the organs and tissues of aquatic organisms, along with Zn magnification across trophic levels in this area [19,35]. Therefore, the dissolved Zn assimilated by aquatic organisms may be partially derived from the internal sediment load. However, the remobilization mechanisms and release characteristics of sediment Zn in this region are currently unknown. Based on the hypothesis that Zn speciation exhibits spatiotemporal variability in sediments because of seasonal hydrological changes driven by surface runoff-tide interactions, the Jiaomen Waterway (JMW; a freshwater–saline water dynamically mixed river) was selected for the exploration of seasonal variations in drivers of sediment Zn mobilization. This study was conducted to determine the impacts of ionic strength on chemical speciation and release potential in sediment; it also quantified the migration features of various Zn species across the SWI.

2. Materials and methods

2.1. Description of study area and sampling sites

The JMW, located in the lower PR basin, South China, has a length of approximately 50 km and water depth of 5–20 m (Fig. 1). This region has a subtropical monsoon climate, with an annual mean temperature of 21.4–22.4 °C and mean precipitation of 1600–2300 mm [25]. The Jiaomen estuary is one of eight major outlets of the PR, with annual runoff constituting 16.8% of the total PR discharge. The study area is covered with unconsolidated quaternary sediments and clay soil ranging

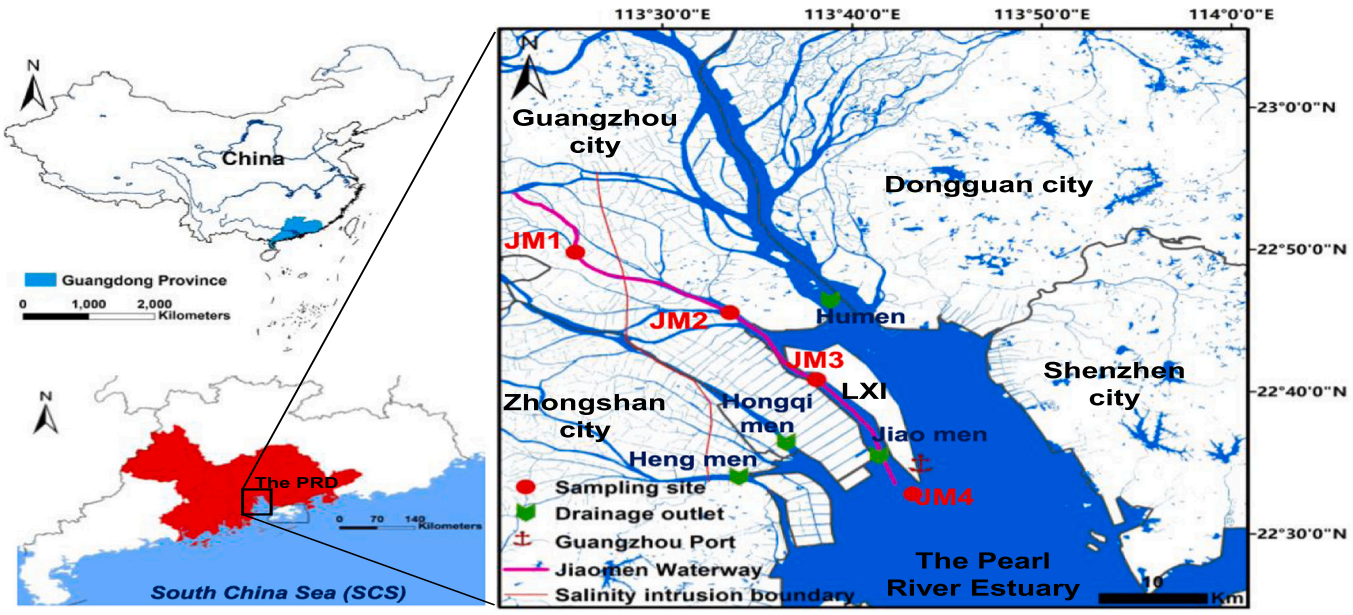

Fig. 1. Location of the study area and sampling sites (The PRD: The Pearl River delta).

from 10 to > 40 m in thickness.

Driven by the irregular semi-diurnal tide of the PR estuary, periodic salinity intrusion considerably alters the hydrochemical characteristics of surface water in the JMW and threatens the safety of upstream water intakes, particularly during dry seasons. Additionally, the PR estuarine region has undergone rapid urbanization, industrialization, and reclamation processes over the past several decades. Large quantities of heavy metals such as Zn have been discharged from industrial effluents, leading to continuous deterioration of surface water quality in the JMW and considerable accumulation of Zn in sediment of the PR estuary [25, 45].

In the present study, site JM1, situated upstream of the salinity intrusion boundary, has hydrochemical properties of freshwater; site JM2 represents the midstream area, where intense brackish water–freshwater interactions occur during the ebb and flood tides, and the hydrochemical type changes frequently. Furthermore, sites JM3 and JM4 are located in the downstream area near Longxue Island (LXI) (Fig. 1), where the fourth largest harbor worldwide, Guangzhou Port, has been in operation for nearly 20 years. The overlying water in this area is generally considered brackish based on previous investigation. The distance between each two sampling sites is approximately 15 km.

2.2. Collection of core sediments

Core sediments including the overlying water were collected using a gravity sampler equipped with a polycarbonate tube (length: 800 mm, inner diameter: 65 mm). Duplicate sediment cores with lengths > 250 mm were obtained at each site during ebb tide in August 2020 and December 2020, representing the summer and winter seasons, respectively. All tubes containing core sediments and overlying waters were immediately wrapped with aluminum foil to protect the samples from sunlight. After transportation to the laboratory, the samples were equilibrated in a thermostatic incubator at 31 °C or 16 °C, as determined during field investigations in summer and winter, for subsequent DGT and HR-Peeper analysis.

2.3. Deployment and measurement of DGT and HR-Peeper probes

DGT and HR-Peeper probes were purchased from www.easysensor.net. DGT probes were used for quantitative determination of DGT-labile Zn, Fe, Mn, and S(-II) in sediment porewater; HR-Peeper probes were used for quantitative determination of dissolved metals in sediment porewater. The deoxygenation, deployment, disassembly, and subsequent pretreatment procedures of DGT probes were extensively described in our previous report [15]. Briefly, Chelex and AgI DGT probes were bound back-to-back and applied to a specific sediment core; the HR-Peeper probe was gradually inserted into another core. All cores containing DGT and HR-Peeper probes were incubated in the dark at a specific temperature, as determined in the field. After 24 h and 48 h of deployment, respectively, DGT and HR-Peeper probes were retrieved and thoroughly rinsed with ultrapure water prior to further analysis. The pretreatment and measurement procedures for the DGT probe are described elsewhere [10,49], and the corresponding calculation processes for DGT and HR-Peeper are summarized in the Supplementary Material (SM).

2.4. Concentration and geochemical fractions of sediment Zn

Approximately 10 mg of freeze-dried and homogenized sediment were weighed in a Teflon tube. An HNO_3—HF mixed solution was used for digestion in a microwave furnace; the resulting digestion solution was diluted to 50 mL with 2% HNO_3 for measurement of the Zn concentration using inductively coupled plasma-mass spectrometry (X-2, Thermo Fisher Scientific, Waltham, MA, USA). The extensively used BCR procedure was adopted to partition the exchangeable and carbonate-bound (F1), reducible (F2), and oxidizable (F3) fractions of sediment Zn. Extraction and analysis details were provided in our previous report [18]. Residual Zn (F4) was determined via subtraction of the first three fractions (F1 +F2 +F3) from the total Zn concentration in sediment. A standard reference material (BCR-701) and method blanks were used for quality assurance and quality control of the extraction procedures and results. The recoveries were 105 ± 1.2% (F1), 104 ± 8.4% (F2), 97 ± 4.8% (F3), 84 ± 3.4% (F4), and 99 ± 1.0% (total Zn). Furthermore, 10% of sediment samples were randomly selected for duplicate analysis, and the standard deviation of analysis results was < 10%.

2.5. Modeling of Zn speciation in water samples

Zn speciation in the overlying water and porewater was simulated using the thermodynamic chemical equilibrium model Visual MINTEQ ver. 3.1 [21]. The input parameters included basic physicochemical

indicators (electrical conductivity, pH, redox potential [E_h], and temperature), major ions (F^-, Cl^-, NO_3^-, SO_4^{2-}, PO_4^{3-}, HCO_3^-, K^+, Na^+, Ca^{2+}, and Mg^{2+}), dissolved organic carbon (DOC), major metals (Fe and Mn), trace metals (Cu, Zn, Ni, Pb, Cd, and Co), and DGT-labile S(-II). The collection and physicochemical analysis of the overlying water and porewater samples are described in the SM. The Stockholm Humic Model assumes a discrete distribution of binding sites and is reportedly capable of describing metal binding across a wide range of conditions [20]. Thus, the Stockholm Humic Model was used to assess competitive interactions of humic substances (HS) with metals in this study. We assumed that HS mainly consisted of fulvic acid (FA) and humic acid (HA), with a total concentration defined as 1.2-fold greater than the DOC concentration [22,38]. For the modeling of Zn speciation in water samples, an FA:HA ratio of 9:1 was used; this ratio is considered representative of conditions in natural waters [22,48]. The default binding constants (log*K*) of Visual MINTEQ were used in this study. The output database includes the concentrations and proportions of various metal species. Furthermore, the saturation index (SI) is automatically calculated to reflect the degree of saturation of a specific mineral phase. A mineral phase reaches oversaturation status in water when SI > 0; otherwise, the mineral phase is considered undersaturated.

2.6. DIFS modeling

The DIFS model is a powerful tool for the quantification of temporal variations in metal concentrations in the dissolved and solid phases in sediment [23]. The depletion extent of metals in porewater caused by DGT uptake can be regarded as a dimensionless ratio (R) (Eq. 1). The simulated time-dependence curve of R is generally used to quantify the capacity for resupply of metals from sediment solids to porewater during DGT deployment. The key parameter is sensitive to the distribution coefficient (K_d, $cm^3 \cdot g^{-1}$) and response time (T_c, s); here, the response time represents the characteristic time required for the perturbed system to reach 63% of its equilibrium condition [23]. In the DIFS model, the adsorption (k_f) and desorption (k_b) rate constants can be estimated based on K_d and T_c (Eqs. 2 and 3).

$$R = \frac{C_{DGT}}{C_{dissolved}} \tag{1}$$

$$K_d = \frac{C_{sediment}}{C_{dissolved}} = \frac{1}{P_c} \times \frac{k_f}{k_b} \tag{2}$$

$$T_c = \frac{1}{k_f + k_b} \tag{3}$$

where P_c is the particle concentration ($g \cdot cm^{-3}$); $C_{sediment}$ and $C_{dissolved}$ are Zn concentrations in the solid phase and dissolved in porewater, respectively ($mg \cdot kg^{-1}$ and $\mu g \cdot L^{-1}$). In this work, the concentration of exchangeable and carbonate-bound Zn (F1) obtained from the BCR procedure was defined as $C_{sediment}$. All parameters required for DIFS simulation are listed in Table S3 of the SM.

2.7. Calculation of Zn exchange flux across the SWI

A benthic exchange flux model based on Fick's first law of diffusion (Eq. 4) [4] was used to identify the direction of Zn migration and quantify its diffusive flux across the SWI. Based on the simulated Zn speciation in the overlying water and porewater, the total Zn flux can be decomposed into the sum of the fluxes of Zn^{2+}, Zn–inorganic, Zn–FA, and Zn–HA complexes (Eq. 5)

$$J = -\varphi D_s \left(\frac{\delta C}{\delta Z}\right)_{(x=0)} \tag{4}$$

$$J = -\varphi \left[D_{s-Ion} \left(\frac{\delta C_{Ion}}{\delta Z}\right)_{(x=0)} + D_{s-Inorg} \left(\frac{\delta C_{Inorg}}{\delta Z}\right)_{(x=0)} + D_{s-FA} \left(\frac{\delta C_{FA}}{\delta Z}\right)_{(x=0)} + D_{s-HA} \left(\frac{\delta C_{HA}}{\delta Z}\right)_{(x=0)} \right] \tag{5}$$

$$D_s = \frac{D_w}{\varphi F} \tag{6}$$

where J is the total diffusive flux across the SWI ($\mu g \cdot m^{-2} \cdot d^{-1}$). $D_{s\text{-}Ion}$, $D_{s\text{-}Inorg}$, $D_{s\text{-}FA}$, and $D_{s\text{-}HA}$ are the diffusion coefficients of free Zn^{2+} ions, Zn–inorganic complexes, Zn–FA complexes, and Zn–HA complexes in sediment ($cm^2 \cdot s^{-1}$), respectively, which can be estimated using Eq. (6) from their diffusion coefficients in water, porosity (φ), and the formation resistivity factor (F) of the sediment ($F = 1/\varphi^3$ when $\varphi \geq 0.7$; otherwise, $F = 1/\varphi^2$) [29]. $(\delta C/\delta Z)_{x=0}$ represents the concentration gradient of each Zn species at the SWI ($\mu g \cdot L^{-1} \cdot cm^{-1}$) and was derived via linear fitting of its vertical distribution between 10 mm above and below the SWI. In this work, the diffusion coefficients of free Zn^{2+} and Zn–inorganic complexes were assumed to be equal in water; they were determined on the basis of temperature, in accordance with the manufacturer's guidelines. $D_{w\text{-}FA}$ and $D_{w\text{-}HA}$ values of 2.46×10^{-6} and 1.79×10^{-6} $cm^2 \cdot s^{-1}$, respectively, in water at 20 °C [48] were used for the determination of $D_{s\text{-}FA}$ and $D_{s\text{-}HA}$.

2.8. Statistical analysis

Because some variables were not normally distributed, the nonparametric Mann–Whitney U test and Kruskal–Wallis H test were used to identify differences in various factors between the two sampling campaigns and among the four sampling sites, respectively. Nonparametric Spearman correlation was used to analyze the relationships among DGT-labile chemicals and between DGT-labile Zn and Zn species predicted using the Visual MINTEQ model. Differences and correlations were considered statistically significant at $p < 0.05$ or $p < 0.01$. Statistical analysis was performed using SPSS software ver. 16.0 for Windows.

3. Results and discussion

3.1. Physicochemical parameters of water and sediment samples

The basic physicochemical parameters of the overlying water, porewater, and sediment samples are presented in Fig. S1 of the SM. Generally, water samples collected from the four sites were slightly alkaline, with mean pH values of 7.32–8.12 across two seasons. Mean values of total dissolved solids (TDS) showed an increasing trend from site JM1 (summer: 0.26 $g \cdot L^{-1}$ and winter: 0.29 $g \cdot L^{-1}$) to JM4 (6.97 and 9.02 $g \cdot L^{-1}$); the substantially higher TDS in winter than in summer was mainly attributed to seasonal dynamic mixing between freshwater and seawater [1]. Based on TDS, the porewater at site JM1 and the downstream sites (JM3 and JM4) was categorized as freshwater (TDS < 1 $g \cdot L^{-1}$) and brackish water (1 $g \cdot L^{-1}$ < TDS < 10 $g \cdot L^{-1}$), respectively [9]. In contrast, the porewater type at site JM2 shifted from freshwater in summer to brackish in winter.

The mean concentrations of dissolved organic carbon (DOC) in porewater showed little variation (7.13–9.27 $mg \cdot L^{-1}$) along the salinity gradient in summer, but they exhibited a distinct decreasing trend from the freshwater (8.80 $mg \cdot L^{-1}$) to brackish water zones (5.00 $mg \cdot L^{-1}$) in winter. OM, which functions as a primary electron donor, was the key factor driving a series of reduction reactions during early diagenesis [11,52]. Compared with site JM4, SO_4^{2-} concentrations were low at sites JM1–JM3 in summer, suggesting strong reduction of sulfates to sulfides and complete depletion of sulfates in porewater [15]; higher SO_4^{2-} concentrations decreased with depth in winter, indicating weaker reduction

of sulfates. These patterns were supported by the redox potential profiles, whereby mean E_h values were substantially lower in summer (−141 to −123 mV) than in winter (−70 to 67 mV) at all sites. Notably, regardless of differences in the E_h profiles at site JM4 obtained during the two sampling campaigns, elevated porewater SO_4^{2-} concentrations (mean: 1570 and 1340 mg·L^{-1}) at that site were attributed to continuous supply from the overlying saline water.

3.2. Distribution characteristics and geochemical partitioning of sediment Zn

The spatial distribution patterns and geochemical fractions of sediment Zn at four sites along the JMW are summarized in Table 1. Total concentrations of sediment Zn (C_{Total}-Zn) were 308 ± 32.3 mg·kg^{-1} at JM1, 220 ± 25.8 mg·kg^{-1} at JM2, 188 ± 13.6 mg·kg^{-1} at JM3, and 122 ± 7.0 mg·kg^{-1} at JM4. A significant decrease in C_{Total}-Zn ($p < 0.05$) was observed with increasing TDS, suggesting a typical pathway of transport from terrestrial sources to the ocean. Previous research has shown that sediment Zn in the PR estuary is mainly derived from industrial effluent discharge, agrochemicals carried in surface runoff, and anti-fouling paints used on cargo ships [37].

According to the modified BCR sequential extraction procedure, acid-soluble (F1), reducible (F2), and oxidizable metals (F3) in sediment are principally related to anthropogenic inputs; they constitute the most mobile geochemical factions [18]. Spatially, Zn in fractions F1, F2, and F3 showed decreasing trends from the upstream to downstream sites; these trends resembled the spatial distribution patterns of C_{Total}-Zn (Table 1), indicating that anthropogenic impacts on the aquatic environment weakened in a manner that increased with migration distance. As shown in Table 1 and Fig. S2, F1 was the dominant fraction of Zn at sites JM1 and JM2, where its mean proportions exceeded 40% of C_{Total}-Zn; the proportions of other fractions at these sites were F2 (20.1% and 20.0%), F4 (18.7% and 24.2%), and F3 (14.7% and 13.7%). Furthermore, the geochemical fractions of Zn followed the order of F4 (47.2% and 67.6%) > F1 (26.6% and 14.2%) > F2 (16.7% and 11.0%) > F3 (9.5% and 7.2%) at sites JM3 and JM4. Based on the BCR partitioning results, the accumulated Zn in sediments, particularly at sites JM1 and JM2, exhibited high mobility potential because metals in F1 are susceptible to desorption from the solid phase through ion exchange and carbonate dissolution under weakly acidic conditions [18]. Regarding the F2 fraction, Zn can be mobilized through the dissolution of Fe and Mn oxides under reducing conditions [12,34]. In the F3 fraction, Zn is mainly bound to OM and sulfides; thus, it is also considered labile during oxidation processes [11,15]. According to the sum of the first three fractions (F1 + F2 + F3) at these sites (Fig. S2), the mobility potential of sediment Zn was in the following order: JM1 > JM2 > JM3 > JM4. However, key influencing factors such as ionic strength (TDS), E_h, and DOC concentrations in porewater showed apparent spatial and seasonal variations (Fig. S1), hindering efforts to identify sources of mobilized metals and the corresponding driving forces. Furthermore, Zn bound to acid-volatile sulfides may be leached during the first extraction step of the BCR procedure [3], inducing considerable augmentation of the F1 fraction of sediment Zn and consequent overestimation of its mobility potential. Therefore, the integration of direct in situ measurement approaches into the determination of metal lability in sediment porewater is strongly recommended for quantitative evaluation of mobility [14].

3.3. Distribution patterns of DGT-labile S(-II), Fe, and Mn

Concentration profiles of DGT-labile S(-II) (C_{DGT}-S(-II)), Fe (C_{DGT}-Fe), and Mn (C_{DGT}-Mn) at the four sampling sites in summer and winter are presented in Fig. 2. In general, C_{DGT}-S(-II), C_{DGT}-Fe, and C_{DGT}-Mn were lower in the overlying water than in sediment porewater. This trend was mainly related to differences in the redox potential of water bodies above and below the SWI. In the oxic overlying water (E_h: 50–105 mV) (Fig. S1), sulfur, iron, and manganese mainly occur in the forms of sulfates and Fe/Mn oxides, which cannot be bound by AgI and Chelex gels, respectively [15,31]. Overall, C_{DGT}-S(-II) was significantly higher in summer than in winter at all sites ($p < 0.05$), confirming that the sediment exhibited more reducing conditions in summer than in winter [15]. At sites JM1 and JM4, the presence of significantly higher C_{DGT}-Fe and C_{DGT}-Mn levels in summer than in winter ($p < 0.05$) could be explained by the more strongly reducing sediment environment (Fig. 2 and S1), which induced greater reductive dissolution of Fe and Mn oxides [34,41]. The opposite seasonal distribution pattern was observed for Fe at site JM2 and for Mn at sites JM2 and JM3; this pattern may be associated with the formation of metal sulfides and diagenesis, because oxidation reactions of ferrous and divalent manganese are not favored in sulfidized sediments [11,31,6]. According to the saturation index (SI) values of Fe- and Mn-bearing minerals in porewater estimated using Visual Minteq (Table S2), iron sulfides were supersaturated, implying the formation of Fe—S minerals such as chalcopyrite ($CuFeS_2$) and pyrite (FeS_2), with respective mean SI values of 19.6–21.4 and 9.9–15.5. Additionally, Mn is preferentially incorporated into the carbonate phase over sulfides in sediments unless the Mn concentration is extremely high [12,24,27]. In the present study, the oversaturation of siderite ($FeCO_3$), rhodochrosite ($MnCO_3$), and amorphous $MnCO_3$ was observed in porewater at sites JM2 and JM3, where mean SI were higher in summer (0.3–1.3) than in winter (0.2–1.1) (Table S1 and Fig. S3). These findings suggested that the formation and precipitation of a series of Fe and Mn carbonates and the associated sulfide minerals were the main drivers, which jointly contributed to decreases in C_{DGT}-Fe and C_{DGT}-Mn in porewater during summer [12,27,6].

3.4. Mobility of sediment Zn determined by DGT analysis

The concentration of DGT-labile Zn (C_{DGT}-Zn) in the overlying water was 43.8–151 μg·L^{-1} in summer and 11.5–98.2 μg·L^{-1} in winter (Fig. 2). Overall, C_{DGT}-Zn substantially decreased from the overlying water to porewater at all sites except JM1 and JM2, which had generally stable concentration profiles in winter. Spatially, C_{DGT}-Zn levels below the SWI were significantly higher at freshwater sites JM1 (32.1 ± 16.8 μg·L^{-1}) and JM2 (43.8 ± 10.7 μg·L^{-1}) than at brackish sites JM3 (25.3 ± 13.3 μg·L^{-1}) and JM4 (29.7 ± 12.9 μg·L^{-1}) in summer ($p < 0.01$); the

Table 1
Total concentration and geochemical fractions of Zn in four sediment cores from the Jiaomen channel (mg·kg^{-1}).

Site	Total concentration	Acid-soluble Zn (F1)	Reducible Zn (F2)	Oxidizable Zn (F3)	Residual Zn (F4)
JM1 ($n = 12$)	308 ± 32.3a	142 ± 13.0a (46.5%)	61.4 ± 5.2a (20.1%)	45.1 ± 6.7a (14.7%)	59.4 ± 29.2 (18.7%)
JM2 ($n = 12$)	220 ± 25.8b	93.2 ± 9.0b (42.7%)	43.7 ± 5.0b (20.0%)	28.5 ± 2.9b (13.1%)	54.2 ± 18.6 (24.2%)
JM3 ($n = 12$)	188 ± 13.6c	49.8 ± 5.0c (26.6%)	31.2 ± 2.1c (16.7%)	17.9 ± 2.0c (9.6%)	88.8 ± 11.6 (48.1%)
JM4 ($n = 12$)	122 ± 7.0d	17.3 ± 2.6d (14.2%)	13.4 ± 2.1d (11.0%)	8.63 ± 0.6d (7.1%)	82.4 ± 7.2 (67.7%)

Data expression: mean ± standard deviation. Data in bracket represents the average percentage of geochemical fraction.
a, b, c, and d indicate significant difference at $p < 0.01$.

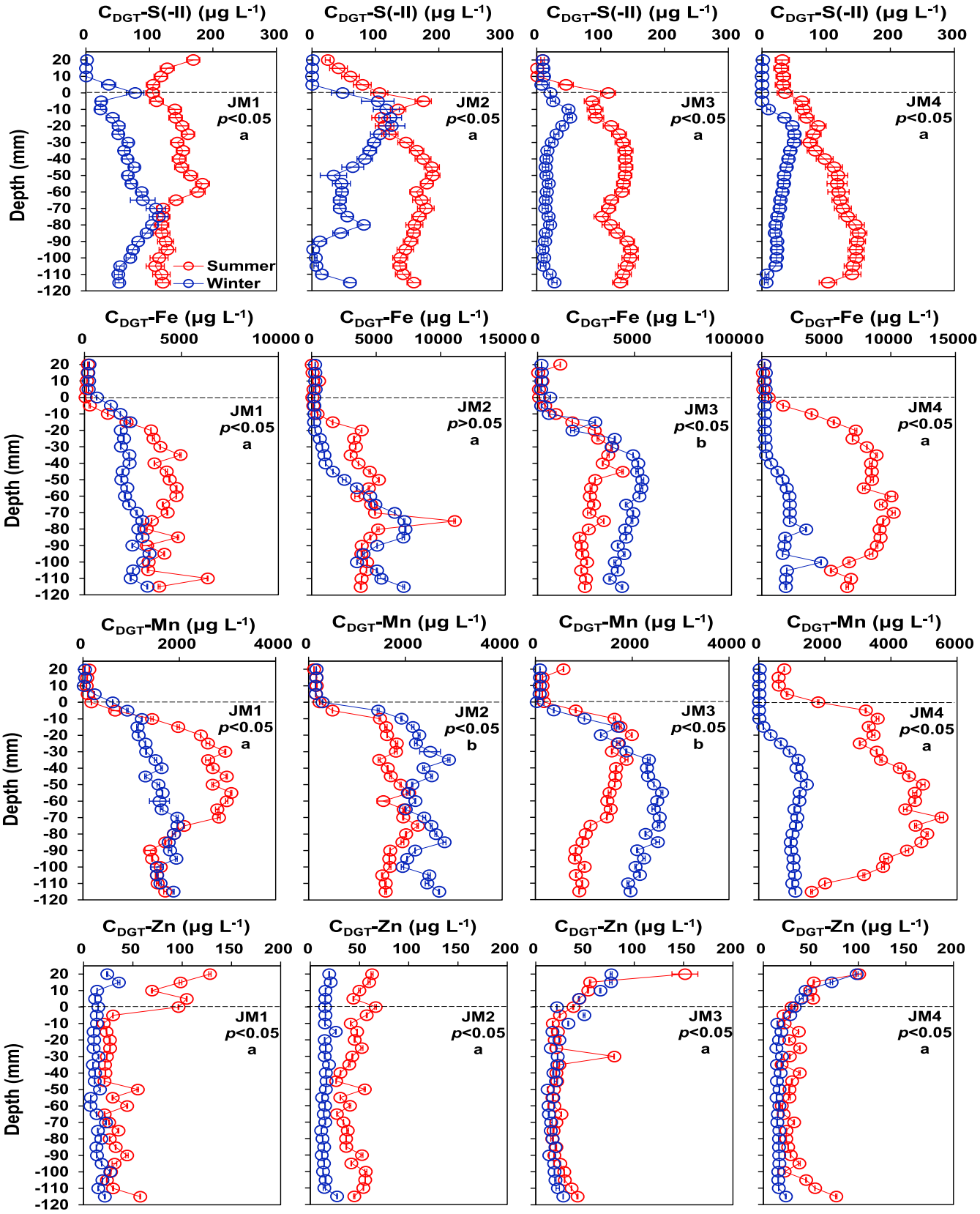

Fig. 2. Seasonal characteristics of DGT-labile chemicals in the overlying water and sediment profiles. Black dashed line represents the sediment-water interface (SWI); a indicates profile of DGT-labile chemicals is higher in summer than in winter, whereas, b represents an opposite situation. Difference is considered significant at $p < 0.05$ based on the nonparametric Mann-Whitney U test.

inverse distribution pattern was observed in winter (JM3 ≥ JM4 > JM2 ≥ JM1, $p < 0.01$) (Table S1), which contradicted the decrease in sediment Zn mobility from the freshwater to brackish zone indicated by BCR analysis. This discrepancy suggests that the potential mobility of sediment Zn cannot be accurately predicted from its geochemical partitioning [44].

DGT-labile Zn exhibited seasonal distribution patterns that were approximately similar to the patterns of Fe, Mn, and S(-II); C_{DGT}-Zn below the SWI was significantly higher in summer than in winter ($p < 0.05$) at all sites (Fig. 2), indicating close relationships associated with seasonal geochemical cycling processes. Previous studies have shown that Fe and Mn oxides generally act as a major sink for sediment metals [15]. In estuarine sediments, Zn is readily desorbed and released from sediment solids through the reductive dissolution of Fe and Mn oxides under anaerobic conditions [12,41]. Furthermore, C_{DGT}-Zn was positively associated with C_{DGT}-Mn ($p < 0.05$) in freshwater sediments, revealing the core role of Mn oxidation–reduction processes in controlling the immobilization and migration behaviors of Zn [26]. Therefore, stronger reductive dissolution of Fe/Mn oxides was presumably the main driver of the higher C_{DGT}-Zn levels observed in sediments under more reducing conditions in summer. However, in this study, C_{DGT}-Zn had negative relationships with C_{DGT}-Fe and -Mn in both seasons ($p < 0.05$ or $p < 0.01$) (Table 2). Notably, porewater Fe and Mn exhibited varying degrees of depletion in both summer and winter because of the formation of sulfide and carbonate minerals (Table S2); in contrast, the opposite distribution patterns of DGT-labile Zn and S(-II) (Table 2) highlighted the non-negligible impacts of S(-II) because Zn-bearing sulfide minerals reached oversaturation and thus insoluble ZnS minerals (e.g., sphalerite [mean SI: 3.6–5.0] and wurtzite [1.4–2.8]; Table S2) tended to be formed in sediments. Additionally, sulfides and carbonates can lower the mobility potentials of divalent metals through sorption and coprecipitation [6]. Thus, the intrinsic coupling of Zn with Fe or Mn may be disrupted by the direct formation of metal-bearing sulfide or carbonate minerals that can adsorb Zn. For these reasons, the reduction of Fe/Mn oxides may not be a reliable proxy for the mobility of sediment Zn in the presence of diagenesis, although reduction of these oxides contributes to the higher C_{DGT}-Zn levels observed in summer.

3.5. Porewater Zn speciation simulated using Visual MINTEQ

As shown in Fig. 3, dissolved Zn concentrations ($C_{dissolved}$-Zn) in the overlying water were in the ranges of 60.4–171 μg·L^{-1} in summer and 19.7–102 μg·L^{-1} in winter. The highest $C_{dissolved}$-Zn value observed at site JM4 exceeded the China Water Quality Standard for Fisheries (100 μg·L^{-1}); thus, it presumably exerted toxic effects on aquatic organisms [33]. The elevated levels of $C_{dissolved}$-Zn suggested the existence of contamination sources such as wastewater discharge around the port of Guangzhou. In porewater samples, the same seasonal distribution characteristics were observed for both dissolved and DGT-labile Zn; concentrations were higher in summer than in winter at all sites ($p < 0.05$) (Figs. 2 and 3). Spatially, $C_{dissolved}$-Zn generally increased with increasing TDS in summer (JM1: 53.3 ± 13.9 ≤ JM2: 63.0 ± 19.1 < JM3: 70.0 ± 36.9 ≤ JM4: 102 ± 25.4 μg·L^{-1}, $p < 0.01$), but it exhibited insignificant differences among sites in winter (means: 27.8–28.8 μg·L^{-1}, $p > 0.05$) (Table 3). Differences in the distribution patterns of $C_{dissolved}$-Zn and C_{DGT}-Zn among sites were presumably related to changes in Zn availability for DGT uptake; such changes were closely associated with the chemical speciation of Zn in porewaters [22,38].

The Zn speciation and relative proportions in water samples are summarized in Fig. 3, Table 3, and Fig. S4. In the overlying water, free Zn ions constituted mean proportions of 61.5% and 57.9% of $C_{dissolved}$-Zn in the summer and winter seasons, respectively, followed by Zn–inorganic (31.6% and 31.0%) and Zn–organic complexes (6.9% and 11.1%). Generally, Zn species were dominated by free ions in the overlying water, which was characterized by low concentrations of sulfides and DOC [2]. Porewater showed an increasing trend of TDS from sites JM1 to JM4, along which the mean proportions of free Zn^{2+} increased from 32.3% to 54.7% in summer and from 12.1% to 52.6% in winter; a similar trend was observed for Zn–Cl complexes, with seasonal proportion ranges of < 0.1–14.4% and < 0.1–13.8%, respectively. In contrast, the proportions of Zn–S complexes, Zn–FA complexes, and Zn–HA complexes decreased with increasing ionic strength, whereas other Zn–inorganic complexes (sum of $ZnOH^+$, $Zn(OH)_{2(aq)}$, $ZnSO_{4(aq)}$, $Zn(SO_4)_2^{-2}$, $ZnCO_3(aq)$, $ZnHCO_3^+$, and $Zn(CO_3)_2^{-2}$) remained stable in the two seasons (14.0–17.6% and 11.5–13.3%, respectively) (Table 3).

At freshwater site JM1, high DOC concentrations (Fig. S1) resulted in the most abundant Zn–organic complexes (sum of Zn–FA and —HA complexes) among all sites, with mean proportions of 48.6% in summer and 70.1% in winter, which are approximately consistent with values measured in riverine sediments (45–85%) [6]. Previous reports have indicated that Zn readily associates with HS such as HA and FA to form organically complexed Zn in the presence of OM in freshwater [53]. At sites JM2–JM4, the increased ionic strength of the porewater would lead to competition for the binding sites of Zn on HS [11,30], inducing the dissociation of Zn–organic complexes. This process may be responsible for the greater proportions of free Zn^{2+} measured in brackish porewaters (Fig. S4). This hypothesis is supported by the formation of Zn–Cl complexes at sites JM2–JM4 and their negligible proportion at site JM1 (< 0.1%) in both seasons (Table 3 and Fig. S4). Additionally, the proportions of Zn–S complexes were approximately reflected by C_{DGT}-S(-II) because Zn preferentially forms its own sulfide mineral (ZnS) at high rates; thus, it is not incorporated into iron sulfide minerals [32]. This absence of Zn from iron sulfide minerals was confirmed based on the oversaturated status of sphalerite and wurtzite in the porewaters of all sites (Table S2). Thus, the greater proportions of Zn–S complexes observed in summer were attributed to the more strongly reducing sediment environment in that season (Table 3 and Fig. S1).

3.6. Relationships between Zn speciation and DGT-labile Zn in porewater

To fully characterize the differences in Zn mobility among the four sites sampled in both seasons, correlations between C_{DGT}-Zn and Zn speciation were analyzed. As shown in Fig. 4a and d, the concentration of free Zn ions was positively correlated with C_{DGT}-Zn in both seasons ($p < 0.05$ or $p < 0.01$). This result was consistent with the design principle of DGT probe that free metal ions are preferentially captured by the Chelex binding gel (Davison and Zhang, 1994). Notably, most data were distributed near or below the 1:1 line, with mean free Zn ion: DGT-labile Zn ratios of 0.32–0.86 in winter; similar distribution patterns were observed for sites JM1 (mean ratio: 0.58) and JM2 (0.73) in summer, suggesting that other Zn species except for Zn^{2+} were available for DGT uptake from porewater. In aqueous environments, free metal ions and inorganically complexed metals are generally regarded as the most labile species that can be directly captured during DGT sampling [51]. With respect to inorganic Zn species, significant positive correlations were observed between the most labile Zn species and C_{DGT}-Zn ($p < 0.05$ or $p < 0.01$) in both seasons (Figs. 4b and 4e). Moreover, all data (with the exception of some data from sites JM3 and JM4) were near the 1:1 line, with high ratios at sites JM1 (0.81) and JM2 (0.96) in summer and at all sites (0.59–1.29) in winter; these findings confirmed that a large

Table 2
Relationships between DGT-labile Zn and Fe, Mn, and S(-II) in water-sediment profiles at four sites in summer and winter.

$n = 112$	Season	C_{DGT}-Fe	C_{DGT}-Mn	C_{DGT}-S (-II)
C_{DGT}-Zn	Summer	-0.242*	-0.408**	-0.106
	Winter	-0.310**	-0.285**	-0.198*

* and ** indicate a significant correlation at $p < 0.05$ and $p < 0.01$, respectively, based on the nonparametric Spearman correlation analysis.

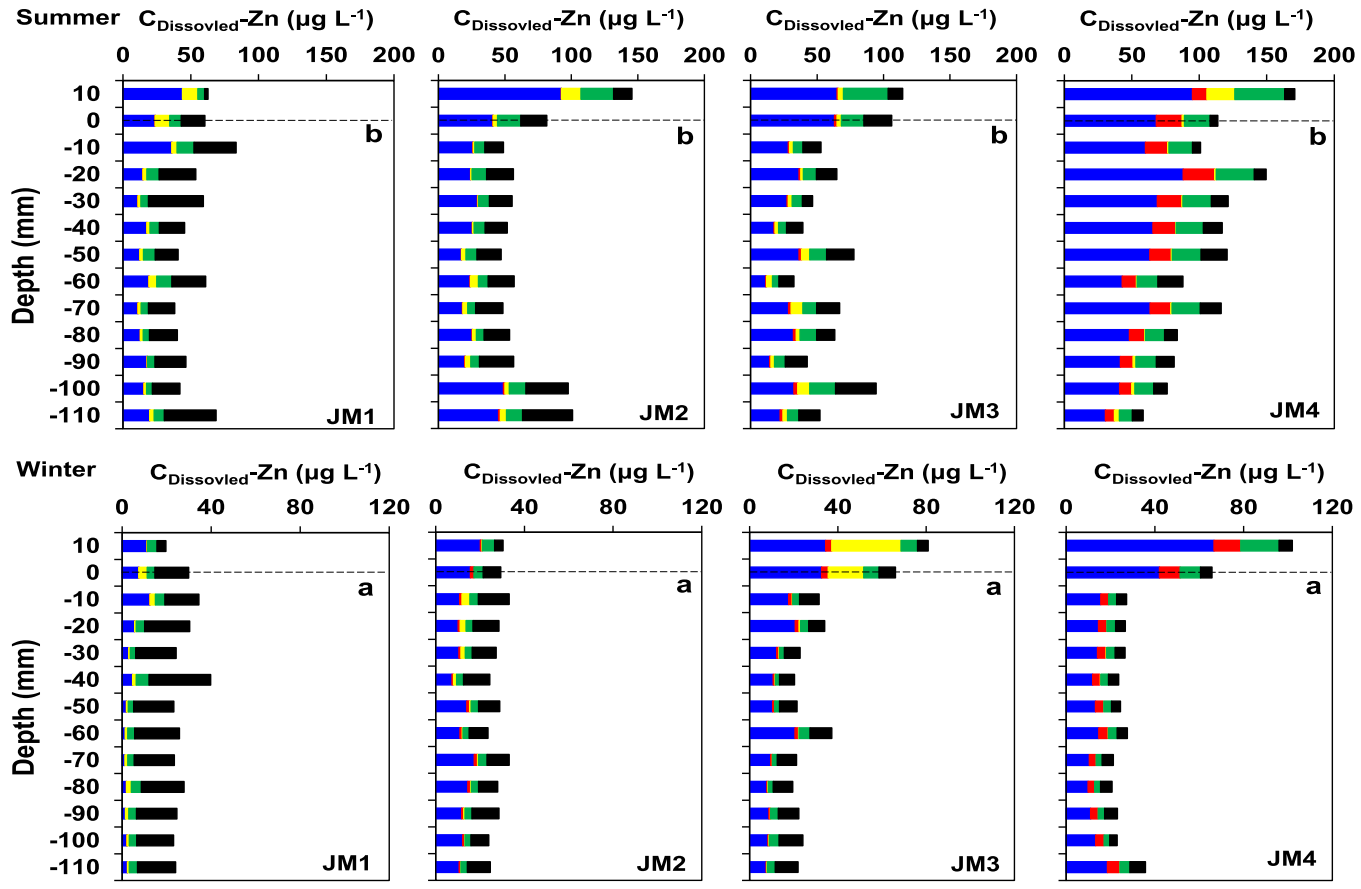

Fig. 3. Seasonal-spatial distribution of free Zn ion, Zn-Cl complexes, Zn-S complexes, other Zn-inorganic complexes, Zn-FA complexes, and Zn-HA complexes predicted with Visual MINTEQ in the sediment porewater at four sites. Black dashed line represents the sediment-water interface (SWI); a and b indicate significant difference between summer and winter seasons at $p < 0.05$. ■Free Zn ion ■Zn-Cl complexes ■Zn-S complexes ■Other inorganic complexes ■Organic complexes.

Table 3
Concentrations of dissolved Zn and percentages of predicted Zn speciation in sediment porewaters ($n = 12$) at four sites in summer and winter.

Site	Season	Dissolved Zn (μg·L^{-1})	Free Zn^{2+}	Zn-Cl complexes	Zn-S complexes	Other inorganic complexes	Zn-FA complexes	Zn-HA complexes
			(%)					
JM1	Summer	53.3 ± 13.9a	32.3 ± 6.8	< 0.1	5.0 ± 2.1	14.0 ± 3.7	43.3 ± 7.7	5.3 ± 1.0
JM2		63.0 ± 19.1a	44.7 ± 6.5	0.7 ± 0.4	4.7 ± 2.9	14.1 ± 2.7	32.0 ± 4.4	3.8 ± 0.6
JM3		70.0 ± 36.9a	45.4 ± 8.7	2.5 ± 0.7	7.6 ± 3.4	16.4 ± 2.3	24.9 ± 5.6	3.0 ± 0.8
JM4		102 ± 25.4b	54.7 ± 3.4	14.4 ± 1.7	1.6 ± 1.7	17.6 ± 0.8	11.3 ± 4.0	1.4 ± 0.5
JM1	Winter	28.4 ± 6.3a	12.1 ± 8.9	< 0.1	4.6 ± 1.8	13.1 ± 2.0	62.3 ± 8.3	7.8 ± 1.1
JM2		27.8 ± 3.3a	42.9 ± 7.9	3.6 ± 0.6	3.8 ± 3.7	11.5 ± 0.5	34.0 ± 5.1	4.3 ± 0.7
JM3		28.6 ± 13.2a	47.3 ± 9.2	3.8 ± 1.1	0.6 ± 0.4	12.3 ± 3.1	32.1 ± 7.6	4.0 ± 1.0
JM4		28.8 ± 12.3a	52.6 ± 3.5	13.8 ± 1.0	1.3 ± 0.7	13.3 ± 1.1	16.9 ± 3.3	2.1 ± 0.4

Data expression: mean ± standard deviation. a, and b indicate significant difference at $p < 0.01$ among four sites in summer and winter.

proportion of the labile Zn determined using DGT was derived from inorganically complexed Zn. For sediments sampled at sites JM3 and JM4 in summer, most data were abnormally distributed above the 1:1 line (Figs. 4a and 4b); this pattern may be associated with the substantially lower C_{DGT}-S(-II) levels compared with the concentrations of dissolved sulfides in brackish porewaters. Previous investigations have shown that the sediment sulfate reduction rate can reach 120 μg·L^{-1}·d^{-1} because of constant replenishment from sulfate-containing overlying brackish water near site JM4, thereby producing levels of acid-volatile sulfides (157–550 mg·L^{-1}; [42,46]) that were three orders of magnitude higher than the values determined using AgI-DGT in the present study (Fig. 2). Thus, the input of lower S(-II) concentrations into the Visual MINTEQ model resulted in underestimation of Zn–sulfide complexes, along with extensive overestimation of free Zn ions, because of the strong binding capacity of sulfides for divalent metal ions [11,41,6]. Overall, negative correlations between organically complexed Zn and C_{DGT}-Zn ($p < 0.01$ or $p > 0.05$) (Figs. 4c and 4f) revealed competitive binding of Zn between Chelex gel and organic complexes, highlighting the suppression of Zn mobility associated with organic complexation. Despite this negative effect of HS in sediments at site JM1, low ratios between the most labile Zn species and C_{DGT}-Zn (summer: 0.81 and winter: 0.59) suggested that organically complexed Zn presumably contributed to the DGT measurement results, because Zn that was weakly bound to organic complexes could become labile and available for DGT uptake through disassociation [22].

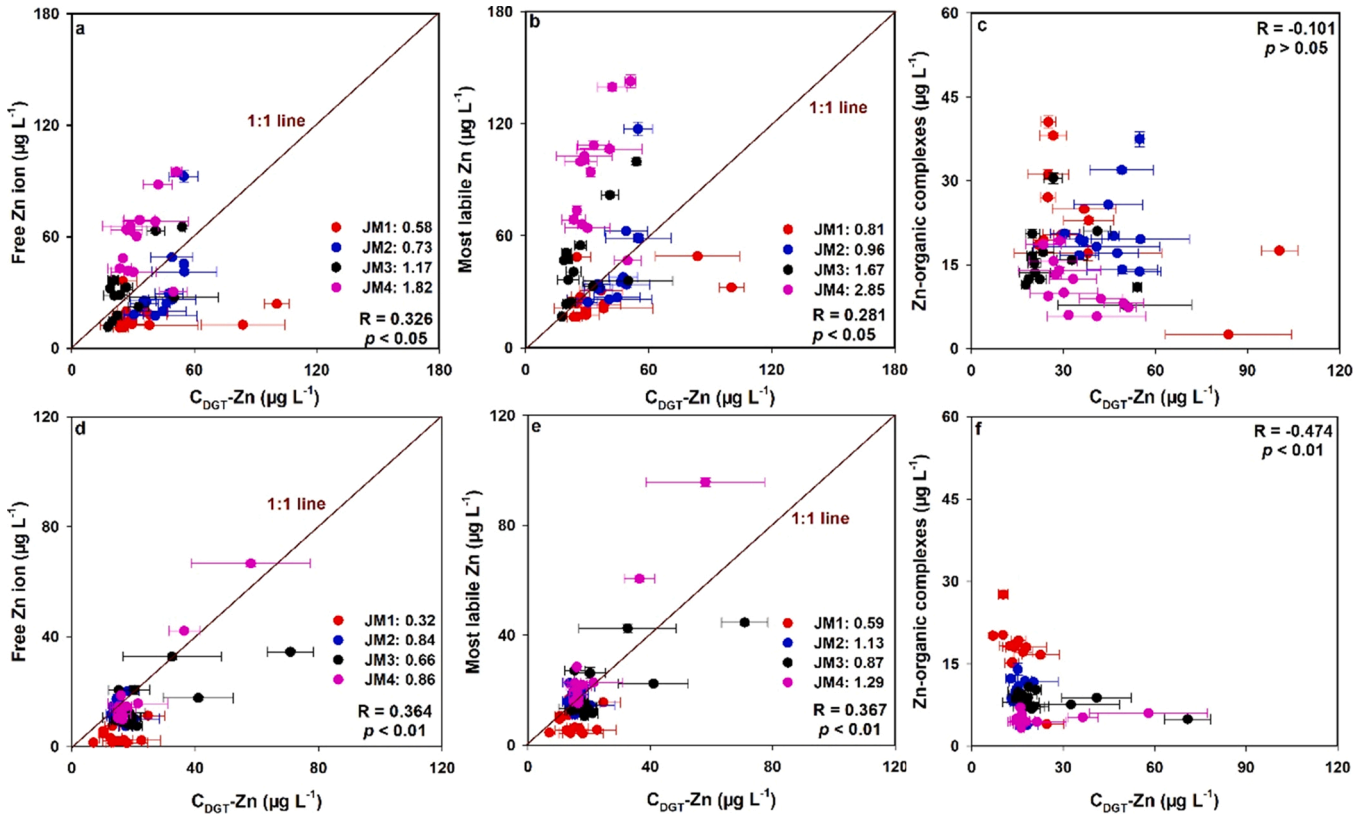

Fig. 4. Correlation between C_{DGT}-Zn and predicted Zn speciation at all sampling sites in summer (a, b, and c) and November (d, e, and f). Most labile Zn represents the sum of concentrations of free Zn ion and Zn-inorganic complexes excluding Zn-S complexes; Zn-organic complexes is the sum of Zn-FA complexes and Zn-HA complexes concentrations; the correlation is significant at $p < 0.05$ or $p < 0.01$.

3.7. Remobilization kinetics of sediment Zn simulated with the DIFS model

The DIFS model was used to simulate the dynamic diffusion and resupply processes of Zn at multiple interfaces of the DGT–porewater–sediment solid system through analysis of calculated parameters such as time-dependent R, response time (T_c), and sorption (k_f)/desorption (k_b) kinetic constants [23]. As shown in Table S3, the resupply model with mean R values of 0.34–0.81 in sediment porewater was regarded as the "partially sustained" case ($0.1 < R < 0.9$) [49], indicating that the depletion of dissolved Zn in porewater because of DGT uptake can be partially buffered by the solid phase of sediment [47]. As shown in Fig. 5, the simulated R values as a function of deployment time by DIFS reached high values within 120 min and subsequently remained constant or gradually decreased (e.g., at JM3 and JM4 in summer). The steeply increasing trend at the beginning of DGT deployment was dependent on the establishment of a linear concentration gradient of diffusing Zn in the diffusive gel located between the porewater and the binding gel. Faster desorption of Zn from the solid phase clearly leads to faster diffusion into the diffusive gel and greater accumulation in the binding gel, thereby shortening the period of increasing R [8]. This tendency was confirmed by the observed k_b–T_c–C_{DGT}–Zn relationships; for example, k_b values were one order of magnitude higher at JM1 (1.61×10^{-5} s^{-1}) and JM2 (1.53×10^{-5} s^{-1}) than at JM3 (1.40×10^{-6} s^{-1}) and JM4 (1.73×10^{-6} s^{-1}) in summer, leading to shorter T_c (941 and 180 s) and higher C_{DGT}-Zn (32.1 and 43.8 μg·L^{-1}) at JM1 and JM2 than at JM3 (2340 s and 25.3 μg·L^{-1}) or JM4 (4850 s and 29.7 μg·L^{-1}). Similar phenomenon was also observed in winter (Tables S1 and S3). Notably, the tendency for R to decrease after its peak at sites JM3 and JM4 in summer reflected the lowered resupply capacity of the solid phase accompanying the sustained uptake of Zn from porewater for DGT sampling; this process could be mainly attributed to the small size of the labile Zn pool (especially F1) in the solid phase (Table 1). As shown in Fig. 5 and Table S3, both the measured R and calculated time-dependence curve of R were higher in summer than in winter at freshwater sites JM1 and JM2. This result was presumably related to the sustained supply of Zn from the solid phase driven by stronger reductive dissolution of Fe/Mn oxides, leading to significantly higher C_{DGT}-Zn (Table S1), although their coupling was likely hidden by diagenesis in the present study (Table S2). This was in accordant with previous research by Yuan et al. [47] who indicated that high R values can be induced by constant desorption because of high concentrations of reducible metals in anaerobic sediments. Whereas, lower R values in winter might be partly associated with scavenging of Zn by newly formed Fe/Mn oxides in the relatively oxic sediments [27]. The opposite seasonal trend was observed at brackish water sites JM3 and JM4, and cation exchange reactions were regarded as the main source of sustained Zn supply at these two sites in winter. Nevertheless, k_f values were 100–10000-fold higher than k_b values at all four sites during both seasons (Table S3), indicating stronger preference for adsorption than for desorption in sediments and confirming the role of sediments as a metal sink in the study area [8,17].

3.8. Source/sink identification and speciation of Zn during migration across the SWI

Exchange fluxes of Zn between sediment and the overlying water were estimated to identify spatial and seasonal source/sink relationships. As shown in Table 4, negative values represent downward migration of Zn from the overlying water to sediment, whereas positive values indicate the release of Zn from the sediment. The total fluxes of Zn at site JM1 were 1.10 μg·m^{-2}·d^{-1} in summer and 8.60 μg·m^{-2}·d^{-1} in winter, indicating that sediments in the freshwater zone acted as a source of Zn to the overlying water. As TDS increased from site JM2 to

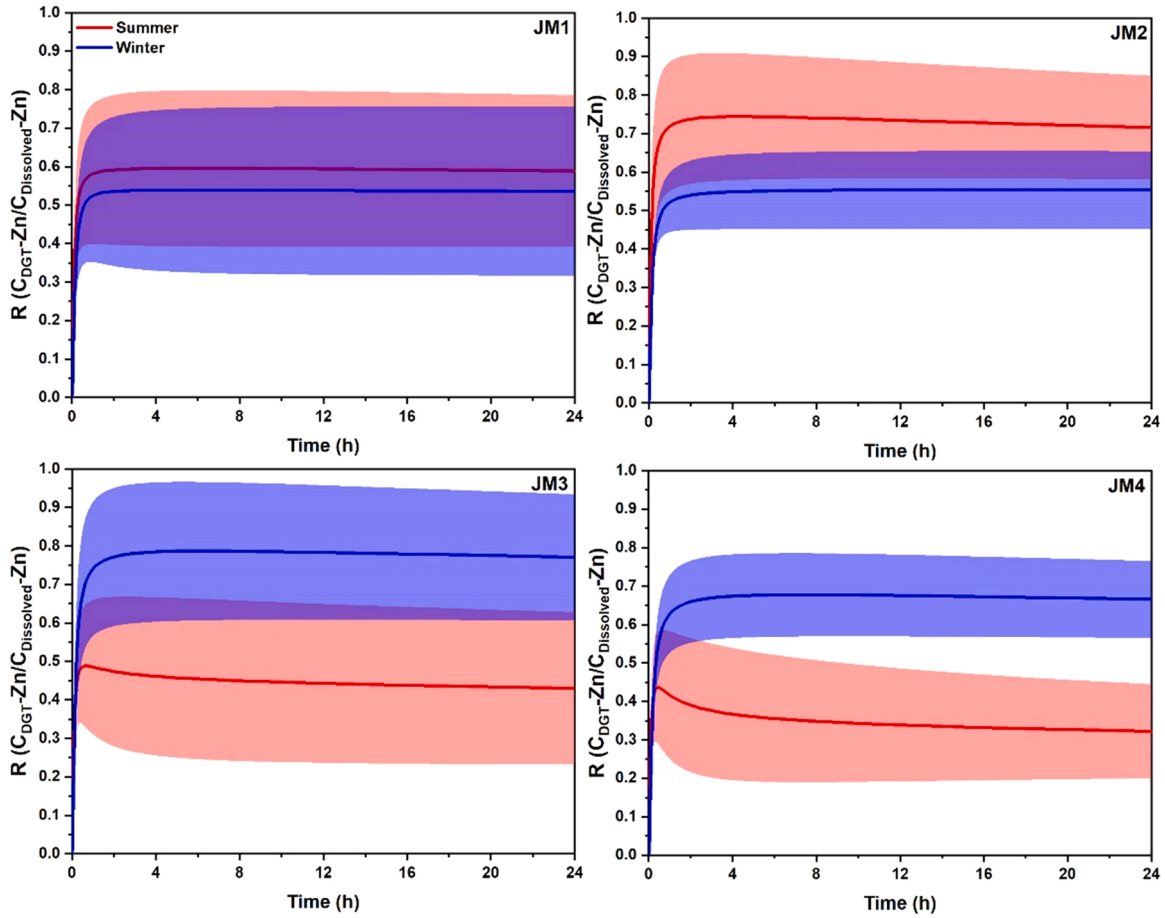

Fig. 5. Time-dependence curve of R values for Zn in the sediments at four sampling sites calculated using DIFS model (Red and blue areas represent the standard deviation in summer and winter, respectively.).

Table 4
Diffusive fluxes of total Zn and its species across the SWI at four sampling sites in two sampling seasons ($\mu g \cdot m^{-2} \cdot d^{-1}$).

Site	Season	Free Zn^{2+}	Zn-inorganic complexes	Zn-FA complexes	Zn-HA complexes	Zn-organic complexes	Total flux
JM1	Summer	-14.5	0.1	14.3	1.23	15.5	1.1
JM2		-118	-54.2	0.2	0.03	0.3	-172
JM3		-62.5	-46.5	1.2	0.1	1.3	-108
JM4		-70.7	-68.3	-0.7	-0.1	-0.8	-140
JM1	Winter	1.3	2.3	4.6	0.4	5.0	8.6
JM2		-13.2	2.7	5.9	0.5	6.4	-4.0
JM3		-18.9	-41.4	1.8	0.2	2.0	-58.4
JM4		-43.5	-18.9	-0.5	-0.1	-0.6	-62.9

Negative values represent a downward migration of Zn from the overlying water to sediment, whereas, positive values indicate the release of sediment Zn.

site JM4, this role changed, such that sediments became a sink with fluxes of −108 to −172 $\mu g \cdot m^{-2} \cdot d^{-1}$ in summer and −4.0 to −62.9 $\mu g \cdot m^{-2} \cdot d^{-1}$ in winter.

Sediment Zn was mainly released as organic complexes into the overlying water at sites JM1–JM3 in both seasons because of high concentrations of DOC in porewater at these sites (Fig. S1). Due to the parameter FA:HA = 9:1 was input into the Visual MINTEQ model, the efflux of FA-complexed Zn, which ranged from 0.2 to 14.3 $\mu g \cdot m^{-2} \cdot d^{-1}$, constituted > 90% of the flux of released Zn–organic complexes, whereas the efflux of HA-complexed Zn was negligible (0.03 to 1.23 $\mu g \cdot m^{-2} \cdot d^{-1}$). As noted above, an increase in ionic strength would promote competition among major cations such as Ca^{2+} for the Zn binding sites of HS in aqueous environments [11,30], thereby enabling the transformation of organically complexed Zn into labile Zn species, followed by migration into the sediment driven by a concentration gradient (Table 4). However, low effluxes of Zn at site JM1 were not the primary reason for elevated influxes of free Zn ions (−18.9 to −70.7 $\mu g \cdot m^{-2} \cdot d^{-1}$) and Zn–inorganic complexes (−18.9 to −68.3 $\mu g \cdot m^{-2} \cdot d^{-1}$) at sites JM3 and JM4, which were one order of magnitude higher than at sites JM1 and JM2. Thus, the discharge of Zn-containing wastewater led to substantial influx of Zn to sediments at downstream sites (Figs. 2 and 3) while contributing to the transport of Zn into estuarine waters.

4. Conclusion

In this work, sediment Zn mobility was assessed using static chemical extraction procedures; the results contradicted the findings obtained by DGT measurement, and the remobilization mechanisms of sediment Zn dynamically differed between seasons. The reductive dissolution of Fe/Mn oxides in the sediments of freshwater zones played a core role in the release of bound Zn during summer, whereas increased ionic strength

promoted Zn desorption from sediment solids and enhanced its mobility in brackish water zones during winter. Assessment of the relationship between labile Zn (determined using DGT) and Zn speciation revealed that, in addition to free Zn ions and Zn–inorganic complexes, Zn weakly bound to organic complexes could also become mobile via disassociation. According to the DIFS modeling results, solid sediment phases showed partially sustained capacity for resupplying Zn to the porewater because of reductive dissolution of Fe/Mn oxides in summer and ion exchange reactions in the brackish water zone in winter. In both summer and winter, sediment functioned as a source of Zn to the overlying water in freshwater zone, but it shifted to become a sink with increasing ionic strength. Importantly, although sediment served as a Zn pool in the brackish water zone, large proportions (> 60%) of labile Zn species were present in porewater, where they posed a potential secondary contamination risk to estuarine waters because of their greater diffusion capacity compared with organically complexed Zn. Finally, enhanced diffusive release of sediment Zn at freshwater sites induced by saline water intrusion in winter deserves concerns.

Environmental Implication

Enrichment of Zn in sediment is potentially toxic to benthic organisms, and diffusive release of sediment Zn likely induces secondary contamination of the water column. However, exploration of its remobilization mechanism remains challenging because of dynamic hydrochemical conditions in estuarine regions. In-situ measurement of Zn speciation in sediment-porewater-water column profiles and estimation of their exchange fluxes at the sediment-water interface were performed in a saltwater-freshwater interzone to identify seasonal variations in remobilization mechanisms of sediment Zn and its interfacial source/sink. We provide new insights into interfacial processes of Zn, highlighting positive effects of salty tide on Zn bioavailability in sediments.

CRediT authorship contribution statement

Lei Gao: Conceptualization, Methodology, Investigation, Writing - Original Draft, Writing - Review & Editing, Funding acquisition, Validation, Project administration. **Rui Li**: Methodology, Investigation, Visualization, Formal analysis, Data curation. **Zuobing Liang**: Investigation, Formal analysis. **Chenchen Yang**: Investigation, Formal analysis. **Zaizhi Yang**: Investigation, Formal analysis. **Lei Hou**: Investigation, Formal analysis. **Lei Ouyang**: Investigation. **Xiuhua Zhao**: Investigation. **Jianyao Chen**: Writing - Review & Editing, Validation, Funding acquisition. **Ping Zhao**: Writing - Review & Editing, Validation.

Declaration of Competing Interest

The authors declare that they have no known competing financial interests or personal relationships that could have appeared to influence the work reported in this paper.

Data availability

Data will be made available on request.

Acknowledgements

This work was financially supported by the National Natural Science Foundation of China (42077376 and 41961144027), the Youth Innovation Promotion Association CAS (2022352), and the Foundation of Key Laboratory of Vegetation Restoration and Management of Degraded Ecosystems, Chinese Academy of Sciences, South China Botanical Garden, Chinese Academy of Sciences (VRMDE2202).

Appendix A. Supporting information

Supplementary data associated with this article can be found in the online version at doi:10.1016/j.jhazmat.2023.131692.

References

[1] Asta, M.P., Calleja, M.L., Perez-Lopez, R., Auque, L.F., 2015. Major hydrogeochemical processes in an acid mine drainage affected estuary. Mar Pollut Bull 91 (1), 295–305.
[2] Balistrieri, L.S., Blank, R.G., 2008. Dissolved and labile concentrations of Cd, Cu, Pb, and Zn in the South Fork Coeur d'Alene River, Idaho: comparisons among chemical equilibrium models and implications for biotic ligand models. Appl Geochem 23 (12), 3355–3371.
[3] Billon, G., Ouddane, B., Boughriet, A., 2001. Artefacts in the speciation of sulfides in anoxic sediments. Analyst 126 (10), 1805–1809.
[4] Blasco, J., Sáenz, V., Gómez-Parra, A., 2000. Heavy metal fluxes at the sediment–water interface of three coastal ecosystems from south-west of the Iberian Peninsula. Sci Total Environ 247, 189–199.
[5] Cantwell, M.G., Burgess, R.M., Kester, D.R., 2002. Release and phase partitioning of metals from anoxic estuarine sediments during periods of simulated resuspension. Environ Sci Technol 36, 5328–5334.
[6] Charriau, A., Lesven, L., Gao, Y., Leermakers, M., Baeyens, W., Ouddane, B., et al., 2011. Trace metal behaviour in riverine sediments: role of organic matter and sulfides. Appl Geochem 26 (1), 80–90.
[7] Chasapis, C.T., Ntoupa, P.A., Spiliopoulou, C.A., Stefanidou, M.E., 2020. Recent aspects of the effects of zinc on human health. Arch Toxicol 94 (5), 1443–1460.
[8] Chen, R., Gao, T., Cheng, N., Ding, G., Wang, Q., Shi, R., et al., 2021. Application of DGT/DIFS to assess bioavailable Cd to maize and its release in agricultural soils. J Hazard Mater 411, 124837.
[9] Costa, M.P.F., Telmer, K.H., 2006. Utilizing SAR imagery and aquatic vegetation to map fresh and brackish lakes in the Brazilian Pantanal wetland. Remote Sens Environ 105 (3), 204–213.
[10] Ding, S., Sun, Q., Xu, D., Jia, F., He, X., Zhang, C., 2012. High-resolution simultaneous measurements of dissolved reactive phosphorus and dissolved sulfide: the first observation of their simultaneous release in sediments. Environ Sci Technol 46 (15), 8297–8304.
[11] Du Laing, G., Rinklebe, J., Vandecasteele, B., Meers, E., Tack, F.M., 2009. Trace metal behaviour in estuarine and riverine floodplain soils and sediments: a review. Sci Total Environ 407 (13), 3972–3985.
[12] Duan, L., Song, J., Liang, X., Yin, M., Yuan, H., Li, X., et al., 2019. Dynamics and diagenesis of trace metals in sediments of the Changjiang Estuary. Sci Total Environ 675, 247–259.
[13] Fang, T., Lu, W., Cui, K., Li, J., Yang, K., Zhao, X., et al., 2019. Distribution, bioaccumulation and trophic transfer of trace metals in the food web of Chaohu Lake, Anhui, China. Chemosphere 218, 1122–1130.
[14] Gao, L., Li, R., Liang, Z., Hou, L., Chen, J., 2021. Seasonal variations of cadmium (Cd) speciation and mobility in sediments from the Xizhi River basin, South China, based on passive sampling techniques and a thermodynamic chemical equilibrium model. Water Res 207, 117751.
[15] Gao, L., Li, R., Liang, Z., Wu, Q., Yang, Z., Li, M., et al., 2021. Mobilization mechanisms and toxicity risk of sediment trace metals (Cu, Zn, Ni, and Pb) based on diffusive gradients in thin films: a case study in the Xizhi River basin, South China. J Hazard Mater 410, 124590.
[16] Gao, L., Li, R., Liang, Z., Yan, C., Zhu, A., Li, S., et al., 2020. Remobilization mechanism and release characteristics of phosphorus in saline sediments from the Pearl River Estuary (PRE), South China, based on high-resolution measurements. Sci Total Environ 703, 134411.
[17] Gao, L., Sun, K., Xu, D., Zhang, K., Gao, B., 2022. Equilibrium partitioning behaviors and remobilization of trace metals in the sediment profiles in the tributaries of the Three Gorges Reservoir, China. Sci Total Environ 849, 157882.
[18] Gao, L., Wang, Z., Li, S., Chen, J., 2018. Bioavailability and toxicity of trace metals (Cd, Cr, Cu, Ni, and Zn) in sediment cores from the Shima River, South China. Chemosphere 192, 31–42.
[19] Gui, D., Yu, R.Q., Karczmarski, L., Ding, Y., Zhang, H., Sun, Y., et al., 2017. Spatiotemporal trends of heavy Metals in Indo-Pacific Humpback Dolphins (Sousa chinensis) from the Western Pearl River Estuary, China. Environ Sci Technol 51 (3), 1848–1858.
[20] Gustafsson, J.P., 2001. Modeling the acid–base properties and metal complexation of humic substances with the stockholm humic model. J Colloid Interface Sci 244, 102–112.
[21] Gustafsson, J.P., 2013. Department of soil and environment. Swed Univ Agric Sci (SLU) (Available at. ⟨https://vminteq.lwr.kth.se/⟩).
[22] Han, S., Naito, W., Hanai, Y., Masunaga, S., 2013. Evaluation of trace metals bioavailability in Japanese river waters using DGT and a chemical equilibrium model. Water Res 47 (14), 4880–4892.
[23] Harper, M.P., Davison, W., Tych, W., 2000. DIFS-a modelling and simulation tool for DGT induced trace metal remobilisation in sediments and soils. Environ Model Softw 15, 55–66.
[24] Herndon, E.M., Havig, J.R., Singer, D.M., McCormick, M.L., Kump, L.R., 2018. Manganese and iron geochemistry in sediments underlying the redox-stratified Fayetteville Green Lake. Geochim Et Cosmochim Acta 231, 50–63.

[25] Huang, L., Bai, J., Xiao, R., Gao, H., Liu, P., 2012. Spatial distribution of Fe, Cu, Mn in the surface water system and their effects on wetland vegetation in the Pearl River Estuary of China. CLEAN Soil Air Water 40 (10), 1085–1092.
[26] Jin, Z., Ding, S., Sun, Q., Gao, S., Fu, Z., Gong, M., et al., 2019. High resolution spatiotemporal sampling as a tool for comprehensive assessment of zinc mobility and pollution in sediments of a eutrophic lake. J Hazard Mater 364, 182–191.
[27] Kalnejais, L.H., Martin, W.R., Bothner, M.H., 2015. Porewater dynamics of silver lead and copper in coastal sediments and implications for benthic metal fluxes. Sci Total Environ 517, 178–194.
[28] Li, R., Liang, Z., Hou, L., Zhang, D., Wu, Q., Chen, J., et al., 2023. Revealing the impacts of human activity on the aquatic environment of the Pearl River Estuary, South China, based on sedimentary nutrient records. J Clean Prod 385, 135749.
[29] Li, Y., Gregory, S., 1974. Diffusion of ions in sea water and in deep-sea sediments. Geochim Et Cosmochim Acta 38, 703–714.
[30] Liu, C., Wang, R., Gao, H., Wu, X., Yin, D., 2022. Transport of trace metals and their bioaccumulation in zooplankton from Changjiang (Yangtze River) to the East China Sea. Sci Total Environ 851 (Pt 1), 158156.
[31] Luo, Y., Ding, J., Shen, Y., Tan, W., Qiu, G., Liu, F., 2018. Symbiosis mechanism of iron and manganese oxides in oxic aqueous systems. Chem Geol 488, 162–170.
[32] Morse, J.W., Luther, G.W., 1999. Chemical influences on trace metal-sulfide interactions in anoxic sediments. Geochim Cosmochim Acta 63, 3373–3378.
[33] Paller, M.H., Harmon, S.M., Knox, A.S., Kuhne, W.W., Halverson, N.V., 2019. Assessing effects of dissolved organic carbon and water hardness on metal toxicity to Ceriodaphnia dubia using diffusive gradients in thin films (DGT). Sci Total Environ 697, 134107.
[34] Parker, R., Bolam, T., Barry, J., Mason, C., Kroger, S., Warford, L., et al., 2017. The application of Diffusive Gradients in Thin Films (DGT) for improved understanding of metal behaviour at marine disposal sites. Sci Total Environ 575, 1074–1086.
[35] Qin, J., Yang, Y., Xu, N., Wang, Q., Sun, X., 2022. Occurrence partition and risk of four adjacent transition metals in seawater sediments and demersal fish from the Pearl River Estuary, South China Sea. Mar Pollut Bull 184, 114159.
[36] Rauch, J.N., Pacyna, J.M., 2009. Earth's global Ag, Al, Cr, Cu, Fe, Ni, Pb, and Zn cycles. Glob Biogeochem Cycles 23 (2) (n/a-n/a).
[37] Shi, C., Chen, J., Gao, L., Gan, H., Xue, Q., Lin, H., 2021. Distribution risk assessment and sources of trace metals in surface sediments from the sea area of Macao, South China. Arch Environ Contam Toxicol 81 (2), 293–306.
[38] Sierra, J., Roig, N., Gimenez Papiol, G., Perez-Gallego, E., Schuhmacher, M., 2017. Prediction of the bioavailability of potentially toxic elements in freshwaters. comparison between speciation models and passive samplers. Sci Total Environ 605–606, 211–218.
[39] Sun, H., Gao, B., Gao, L., Xu, D., Sun, K., 2019. Using diffusive gradients in thin films (DGT) and DGT-induced fluxes in sediments model to assess the dynamic release of copper in sediment cores from the Three Gorges Reservoir China. Sci Total Environ 672, 192–200.
[40] Tang, W., Duan, S., Shan, B., Zhang, H., Zhang, W., Zhao, Y., et al., 2016. Concentrations diffusive fluxes and toxicity of heavy metals in pore water of the Fuyang River, Haihe Basin. Ecotoxicol Environ Saf 127, 80–86.
[41] Wang, W., Wang, W.X., 2017. Trace metal behavior in sediments of Jiulong River Estuary and implication for benthic exchange fluxes. Environ Pollut 225, 598–609.
[42] Wu, Z., Zhou, H., Peng, X., Chen, G., 2006. Anaerobic oxidation of methane: geochemical evidence from pore-water in coastal sediments of Qi'ao Island (Pearl River Estuary), southern China. Chin Sci Bull 51 (16), 2006–2015.
[43] Xu, D., Gao, B., Gao, L., Zhou, H., Zhao, X., Yin, S., 2016. Characteristics of cadmium remobilization in tributary sediments in Three Gorges Reservoir using chemical sequential extraction and DGT technology. Environ Pollut 218, 1094–1101.
[44] Xu, Q., Gao, L., Peng, W., Gao, B., Xu, D., Sun, K., 2018. Assessment of labile Zn in reservoir riparian soils using DGT, DIFS, and sequential extraction. Ecotoxicol Environ Saf 160, 184–190.
[45] Ye, Z., Chen, J., Gao, L., Liang, Z., Li, S., Li, R., et al., 2020. ^{210}Pb dating to investigate the historical variations and identification of different sources of heavy metal pollution in sediments of the Pearl River Estuary, Southern China. Mar Pollut Bull 150, 110670.
[46] Yin, X.J., Zhou, H.Y., Yang, Q.H., Sun, Z.L., 2010. Sulfate reduction and reduced sulfur speciation in the coastal sediments of Qi'ao Island in the Zhujiang Estuary in China. Acta Oceanol Sin 32, 31–39.
[47] Yuan, H., Yin, H., Yang, Z., Yu, J., Liu, E., Li, Q., et al., 2020. Diffusion kinetic process of heavy metals in lacustrine sediment assessed under different redox conditions by DGT and DIFS model. Sci Total Environ 741, 140418.
[48] Zhang, H., 2004. In-situ speciation of Ni and Zn in freshwaters: comparison between DGT measurements and speciation models. Environ Sci Technol 38, 1421–1427.
[49] Zhang, H., Davison, W., Knight, B., Mcgrath, S., 1998. Situ measurements of solution concentrations and fluxes of trace metals in soils using DGT. Environ Sci Technol 32, 704–710.
[50] Zhang, H., Zhao, Y., Wang, Z., Liu, Y., 2021. Distribution characteristics bioaccumulation and trophic transfer of heavy metals in the food web of grassland ecosystems. Chemosphere 278, 130407.
[51] Zhang, J.Z., Millero, F.J., 1994. Investigation of metal sulfide complexes in sea water using cathodic stripping square wave voltammetry. Anal Chem Acta 284, 497–504.
[52] Zhang, L., Wang, L., Yin, K., Lü, Y., Zhang, D., Yang, Y., et al., 2013. Pore water nutrient characteristics and the fluxes across the sediment in the Pearl River estuary and adjacent waters, China. Estuar Coast Shelf Sci 133, 182–192.
[53] Zhu, Y., Gueguen, C., 2016. Evaluation of free/labile concentrations of trace metals in Athabasca oil sands region streams (Alberta, Canada) using diffusive gradient in thin films and a thermodynamic equilibrium model. Environ Pollut 219, 1140–1147.